Geophysical Research Letters®

Author Contributions:

Conceptualization: Tomoya Takano, Kiwamu Nishida
Data curation: Tomoya Takano, Kiwamu Nishida
Formal analysis: Tomoya Takano
Funding acquisition: Tomoya Takano
Investigation: Tomoya Takano
Methodology: Tomoya Takano, Kiwamu Nishida
Resources: Tomoya Takano, Kiwamu Nishida
Software: Tomoya Takano, Kiwamu Nishida
Supervision: Kiwamu Nishida

Tidal Response of Seismic Wave Velocity at Shallow Crust in Japan

Tomoya Takano[1] and **Kiwamu Nishida[2]**

[1]Graduate School of Science and Technology, Hirosaki University, Hirosaki, Japan, [2]Earthquake Research Institute, The University of Tokyo, Tokyo, Japan

Abstract Microcracks in geomaterials cause variations in the elastic moduli under applied strain, thereby creating seismic wave velocity variations. These are crucial for understanding the dynamic processes of the crust, such as fault-zone damage, healing, and volcanic activities. Solid earth tides have been used to detect seismic velocity changes responding to crustal-scale deformations. However, no prior research has explored the characteristics of the seismic velocity variations caused by large-scale tidal deformation. To systematically evaluate the tidal response to velocity variations, we developed a new method that utilized the flexibility of a state-space model. The tidal response was derived from hourly stacked noise autocorrelations using a seismic interferometry method throughout Japan. In particular, large tide-induced seismic velocity changes were observed in the low S-wave velocity region of the shallow crust. Overall, the tidal responses of velocity variations can provide new insights into the response mechanisms of the shallow crust to applied strain.

Plain Language Summary Rock deformations can open or close microcracks in rocks along with varying their elastic moduli under an applied strain. The temporal variations in the elastic moduli of rocks alter the seismic wave velocity, which can be monitored to provide information on the strain applied to the crust. This is crucial for understanding the geological processes in fault zones and volcanic regions. To utilize the seismic velocity variations for monitoring how much the Earth's structure deforms, the response of the seismic velocity to the deformations must be assessed. The deformation of the Earth's surface caused by lunar and solar gravity, called solid Earth tides, has been used to study seismic velocity variations in response to crustal deformation. However, only a limited number of regions have been studied for the tidal response of the seismic velocity, and the characteristics of its variations caused by tidal deformation were not yet apparent. This study measured the tidal responses to seismic velocity variations throughout Japan with reliable estimations. Notably, the tide-induced seismic velocity variations tend to increase in the low S-wave velocity region. Overall, these results provide new insights into the response mechanisms of the shallow crust to deformations.

1. Introduction

The temporal evolution of the strain applied to the crust is essential for understanding the dynamic processes in fault zones and active volcanoes. Earthquakes depend on the strain state of the Earth and the fluid distribution around the fault, while volcanic eruptions occur because of the pressure accumulation under volcanic fluid pressurization and magma supply from deeper regions. Upon observing the crustal response to the applied strain, the in-situ strain variations in the crust can be estimated, which generally involve limitations in the case of direct measurement. The geomaterials in the crust are nonlinearly elastic (Walsh, 1965), and their elastic moduli vary with the applied strain. As the seismic wave velocity depends on the elastic moduli, the applied strain induces variations in the seismic wave velocity. Specifically, the opening and closing of cracks or pores in rock according to the strain changes cause the seismic velocity to decrease and increase, respectively. Therefore, tracking the seismic wave velocity variations can adequately serve as a proxy for examining the temporal variations in the elastic constants caused by the applied strain in the crust. Previous studies have reported that the temporal variations in the seismic wave velocity are associated with the static strain variations induced by, for instance, large earthquakes (e.g., Brenguier, Campillo, et al., 2008) and volcanic activities (e.g., Brenguier, Shapiro, et al., 2008; Takano et al., 2017). To monitor the applied strain in the crust and its responses, the variations in the seismic wave velocity response to a given strain perturbation must be examined.

As we can precisely compute the static strain caused by a solid earth tide, the seismic velocity variations associated with the tidal strain provide information on the strain–velocity relationships on Earth. Earlier studies have

Validation: Tomoya Takano
Visualization: Tomoya Takano
Writing – original draft: Tomoya Takano
**Writing – review & editing:** Tomoya Takano, Kiwamu Nishida

shown that controlled active seismic experiments observed decrease and increase in velocity associated with the opening and closure of cracks in the subsurface due to tide (e.g., De Fazio et al., 1973; Reasenberg & Aki, 1974; Yamamura et al., 2003). However, active seismic experiments do not yield temporal resolution and constrained locations in repeated experiments. Recently, a passive noise-based technique (e.g., Obermann & Hillers, 2019) observed seismic velocity variations related to tides (e.g., Hillers et al., 2015; Mao et al., 2019; Sens-Schönfelder & Eulenfeld, 2019; Takano et al., 2014, 2019). To estimate the velocity variations caused by tides, two strategies have been employed using ambient noise correlations. The first one involves stacking ambient noise correlations according to the tidal deformation amplitude and measuring the phase differences between the noise correlations during crustal dilatation and contraction (Hillers et al., 2015; Takano et al., 2014, 2019). By stacking the noise correlations for a long time-period, the velocity variations caused by the nontidal effects can be canceled. The second one examines velocity variations corresponding to tidal harmonics from the spectrum of seismic velocity variations with high temporal sampling (Sens-Schönfelder & Eulenfeld, 2019). These previous studies estimated the strain–velocity sensitivities based on the velocity variations induced by tidal deformation at depths shallower than a few kilometers. As such, the strain–velocity sensitivity may depend on the strength of nonlinear elasticity at their location. The tidal responses of velocity variations have been detected in limited regions, but the spatial features of the seismic velocity variations in response to crustal-scale tidal deformation have not been reported. To estimate the spatial distribution of velocity changes in response to tides, it is necessary to measure the response using a uniform method and establish criteria for determining whether the seismic wave velocity responds to tides. This study aims to calculate the tidal response of the velocity variations in the shallow crust throughout Japan for proposing the criteria for detecting these tidal responses.

Accurately separating tidal responses from other causes of seismic velocity variations is essential for estimating tidal strain-related variations in seismic velocity. Recently, Nishida et al. (2020) developed a novel method for estimating seismic velocity variations. They utilized an extended Kalman filter based on a state-space model (e.g., Durbin & Koopman, 2012), to estimate the seismic velocity variations as a state variable and used the Maximum Likelihood method to estimate the hyperparameters. The flexibility of the state-space model for the time-series data can easily incorporate the seismic wave velocity variations induced by external perturbations into the model. As the period, phase, and amplitude of the tides were accurately determined in advance, the superposition of the periodic functions can model the tide-induced velocity variations. Thus, the tidal responses of the velocity variations were incorporated into the state-space model as hyperparameters, allowing for the systematic estimation of tidal strain response using the extended Kalman filter and Maximum Likelihood method.

We investigated seismic velocity variations in response to tidal strains throughout Japan. Using Japan's dense seismic network, we calculated the causal part of nine components of the ambient-noise autocorrelation functions. We then extracted the seismic velocity variations related to the tide from the hourly stacked-noise correlations using an extended Kalman filter with a Maximum Likelihood method. We compared the observed strain–velocity sensitivities with the S-wave velocity structure to better understand the mechanical properties of the shallow crust under deformation.

2. Data

We computed autocorrelation functions of ambient noise at a single station using 796 Hi-net seismic stations operated by the National Research Institute for Earth Science and Disaster Prevention (NIED). The use of borehole-type sensors in most Hi-net ensures that the characteristics among instruments vary minimally. The location map of the seismic stations with the maximum tidal volumetric strain at the ground surface computed by GOTIC2 (Matsumoto et al., 2001) is illustrated in Figure 1. GOTIC2 computes the tidal strain, including the solid earth tide and ocean load. The GOTIC2 program computed ocean loading with a five-minute resolution around Japan. The NIED deployed three-component velocity meters with a natural frequency of 1 Hz at the bottom of each borehole located at a depth of about 100 m or more at most stations. After subtracting the common data logger noise, which was obtained by stacking waveforms of all Hi-net stations every minute (Takagi et al., 2015), the instrumental responses of the seismometers were deconvolved using the inverse filtering technique (Maeda et al., 2011). We resampled the data to 2 Hz to efficiently compute the correlation functions. For each station every hour, we computed three components (north-north, east-east, upward-upward) of an auto-correlation function and three components (east-north, east-upward, and north-upward) of a single-station cross-correlation (Hobiger et al., 2014). We used the causal part of the nine components of correlation. The correlation functions
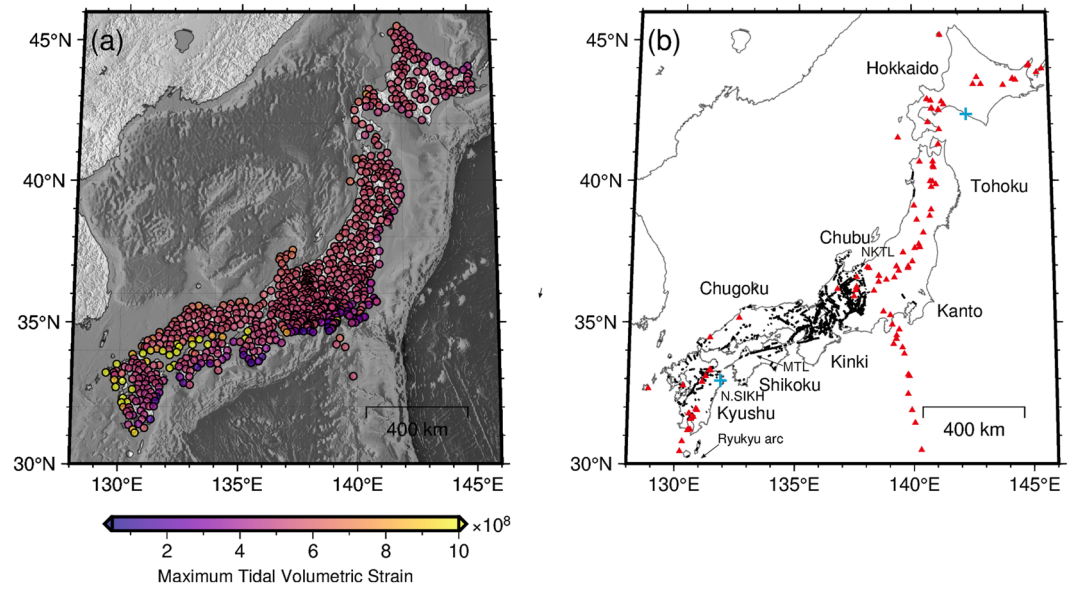
Figure 1. (a) Location map of seismic stations. The color scale displays the maximum volumetric tidal strain. (b) Geological features in Japan. Red triangles display active volcanoes; solid-black lines represent active faults (Nakata & Imaizumi, 2002); the blue symbol indicates the location of N.SIKH.

were filtered at frequency bands of 0.2–0.5 Hz. In summary, we analyzed the ambient noise recorded from 1 January 2010, to 31 December 2011.

3. Method

The tidal response of seismic velocity variations was determined from the hourly stacked noise correlations using the extended Kalman filter with the Maximum Likelihood method based on the state-space model (Nishida et al., 2020). In Kalman filter processing, we minimized the squared differences between the model correlation function predicted from one previous step and the observed correlations. Assuming that the temporal variations of the seismic wave velocity in a given medium occur homogeneously, a model function of the observed correlations can be expressed by altering the amplitude and stretching factor of the reference correlation function using a stretching method in the time domain (Weaver & Lobkis, 2000). The stretching method has been linearized for application to a Kalman filter (Nishida et al., 2020). The tidal response of the velocity variations was determined as the explanatory variables in a state-space model in two steps. First, the temporal variations of amplitude and the stretching factor of the correlations were estimated as state variables in a state-space model with Kalman Filter processing. Second, the tidal response of the velocity variations was determined as an explanatory variable, referred to as a hyperparameter, using the Maximum Likelihood method. We could evaluate with statistical criteria even at stations where the tidal response of velocity changes was not clearly observable using the likelihood computed during the process. Thus, we constructed a state-space model as follows:

$$ \boldsymbol{y}_t^p = \boldsymbol{m}^p(\boldsymbol{\alpha}_t + \boldsymbol{R}_t) + \boldsymbol{\epsilon}_t, \qquad \boldsymbol{\epsilon}_t \sim \mathcal{N}(0, \boldsymbol{H}_t) \tag{1} $$

$$ \boldsymbol{\alpha}_{t+1} = \boldsymbol{\alpha}_t + \boldsymbol{\eta}_t, \qquad \boldsymbol{\eta}_t \sim \mathcal{N}(0, \boldsymbol{Q}_t), \tag{2} $$

where $\boldsymbol{y}_t^p$ denotes the data vector of the observed correlations for the p th component ($\boldsymbol{m}^p$), $\boldsymbol{\alpha}_t$ represents the state vector containing the stretching factor and amplitude of correlations, $\boldsymbol{R}_t$ symbolizes the explanatory variable related to the tides, and $\boldsymbol{\epsilon}_t$ and $\boldsymbol{\eta}_t$ indicate the mutually independent random variables subject to a normal distribution ($\mathcal{N}$) with zero means and covariance matrix $\boldsymbol{H}_t$ and $\boldsymbol{Q}_t$, respectively. The state-space model enables the procedure to handle missing values as unknown random variables. The Equations 1 and 2 have been elaborately expressed in Supporting Information S1 (refer to Text S1).

To compute the reference correlation at each station, we estimated the state variables of the stretching factor and amplitude common across all nine components without any explanatory variables. Thereafter, the reference

correlation was estimated by averaging the observed correlations stretched with the estimated amplitude and stretching factor for the observation duration. Prior data covariance, h_0, was estimated based on the time average of the squared differences between the observed and reference correlations. The validation of prior data covariance is described in the Supporting Information S1 (Text S2). The state variables were estimated through the recursive linear Kalman filter and smoother (Durbin & Koopman, 2012) by adjusting the explanatory variables, initial stretching factor, and prior model covariance for the initial value.

The tidal response of the seismic wave velocity was modeled by adding the cosine functions related to the tidal constituents as follows:

$$r_t = \sum_{m=1}^{M} A_m \cos(\omega_m t + \varphi_m + \theta_m) \tag{3}$$

where m denotes the index of the tidal constituents, A_m indicates the sensitivity of the seismic wave velocity to tidal strain, φ_m represents the phase angle of the tide, ω_m denotes the angular frequency of the tide, and θ_m represents the difference between the tidal strain and the observed variations in seismic velocity. A phase delay may occur in the response of the velocity variations to tidal strain caused by the nonlinear elasticity of the rock (Sens-Schönfelder & Eulenfeld, 2019). φ_m was estimated from the theoretical tidal strain computed using GOTIC2 at each station, whereas ω_m was obtained from the table of tidal constituents (Cartwright & Edden, 1973). The velocity variations related to only M_2 tide were incorporated into the modeled tidal response of the seismic wave velocity, which most significantly contributed to the seismic wave velocity variations in the tidal constituents (Sens-Schönfelder & Eulenfeld, 2019). As the M_2 tide originated from the moon, the thermoelastic effects did not contribute to the seismic velocity variations.

The logarithmic likelihood $\ln L$ was maximized with respect to the hyperparameters. $\ln L$ was computed following the Kalman filtering processes (e.g., Durbin & Koopman, 2012); $\ln L$ is a function of hyperparameter β as

$$\beta = \left(p_0, p_1, \gamma_1, A_{M_2}, \varphi_{M_2}\right), \tag{4}$$

where p_0 and p_1 represent the covariance of the initial value of the amplitude and stretching factor, respectively, γ_1 denotes the initial value of the stretching factor, and A_{M_2} and φ_{M_2} denote the tidal strain-velocity sensitivity and phase shift between the tidal strain and velocity variations for the M_2 tide, respectively. The covariance of the initial value was assumed to be equal to that of the prior model. Using the quasi-Newton method (Zhu et al., 1997), the logarithmic likelihood $\ln L$ was maximized with respect to the hyperparameters, searching for tidal strain responses from 0.001 to 1 % and phase shift from $-180°$ to $180°$, respectively. In our tidal response model, we considered only velocity decrease and increase caused by the opening and closing of micro-cracks due to strain changes. The negative strain-velocity sensitivity can be explained by a phase shift of approximately 180°. Considering a large covariance of the stretching parameter creates large short-term variations in seismic wave velocity, which could mask the negligible velocity variations induced by the tides. We set the search range of p_1 to account for long-term seasonal variations and short-term tidal responses. In particular, p_1 ranging from 2×10^{-13} to 5×10^{-10} varied the stretching parameters from 0.0001% to 0.05% linearly for 3 hours, whereas they were estimated up to 1% for 1 month. We present here a case of the significant tidal response of velocity changes observed at the N.SIKH station. Figures 2a and 2b show the time series of the observed velocity variations without the explanatory variables. The long-term velocity variations ranged from a few days to tens of days (Figure 2a). A half-day cycle was observed in the velocity variations occurring over a few days (Figure 2b). The power spectrum of the 2-year seismic wave velocity estimated without the explanatory variables displayed a spectral peak corresponding to the semi-diurnal tidal variation (Figure 2c). With the Maximum Likelihood method applied to determine the velocity variation related to the M_2 tide as an explanatory variable, the tidal response was estimated with statistical reliability. In Figure 2d, the spectral peak of the velocity variations during the period of M_2 tide disappeared because the velocity variation caused by M2 tide was extracted as the explanatory variable.

To evaluate whether the observed velocity variations reliably respond to the tide, the appropriate number of hyperparameters was estimated using the Akaike Information Criterion (AIC) (Akaike, 1974) defined as

$$AIC_K = -2\ln \hat{L}_K + 2K \tag{5}$$

where K denotes the number of hyperparameters and $\ln \hat{L}_K$ represents the logarithmic likelihood for K hyperparameters. We compared the AIC between the hyperparameters, including the tidal response of the velocity variations. If the increment of AIC ($\Delta AIC \equiv AIC_K - AIC_{K-2}$) was less than zero, the hyperparameters, including
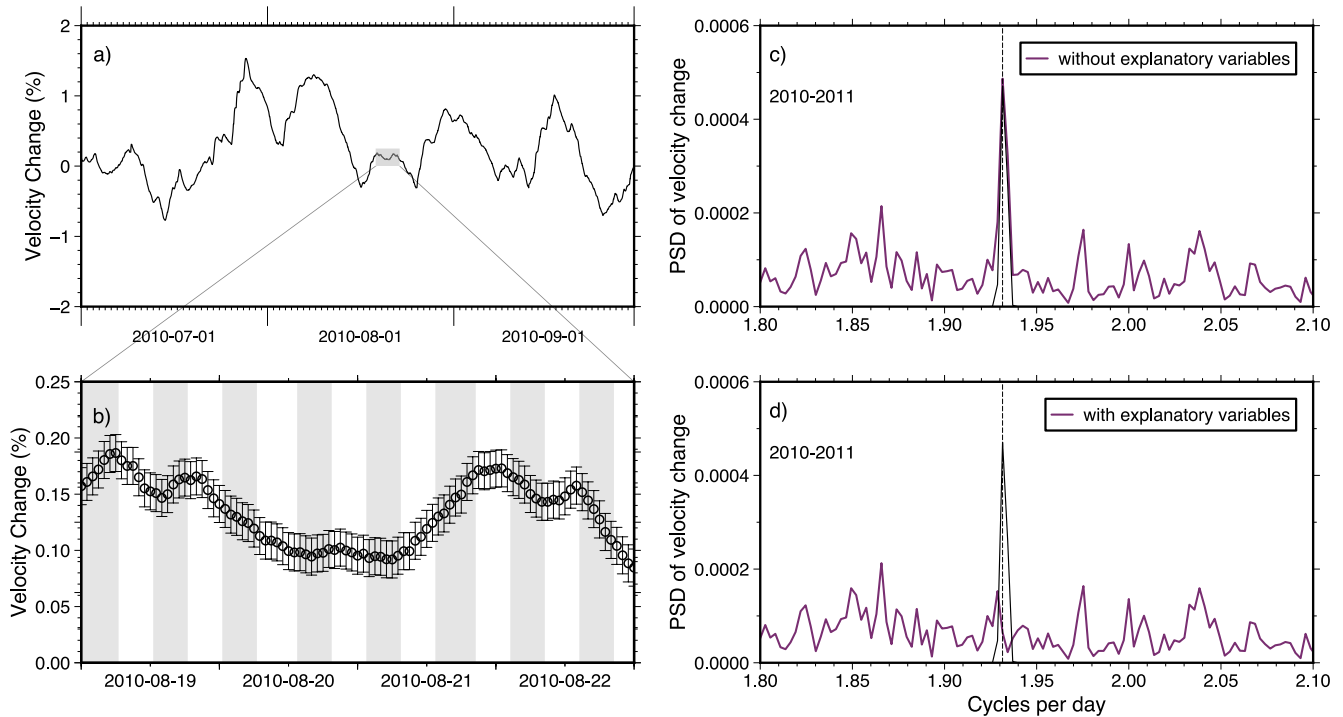
Figure 2. (a) Time series of velocity variations estimated without explanatory variables from 2010/7/1 to 2010/9/30 at N.SIKH station. (b) Enlarged view of the shaded region in Figure (a). The gray region depicts the period of contraction under M_2 tide. (c) The purple line denotes the power spectrum of velocity variations (%^{2}/cycles per day). The black line displays the power spectrum of modeled velocity variations. Dashed-black line represents the cycles per day of the M_2 tide. The power spectrum was computed for the observed duration. (d) Power spectrum of velocity variations (%^{2}/cycles per day) with the explanatory variables. The black line indicates the power spectrum of modeled velocity variations. Dashed-black line denotes the cycles per day of the M_2 tide.

M_2 tides, were deemed as appropriate. Among all stations, 56.5% of the stations displayed a reliable tidal response to the velocity variations.

4. Results

Figure 3 illustrates the spatial distribution of the velocity variations in response to M_2 tide The velocity variations in response to the M_2 tide were estimated up to 0.35%. At stations with ΔAIC greater than 0, the velocity variations were generally estimated as less than 0.001%, indicating that the tidal response to the velocity variations was not statistically significant (Figure S2 in Supporting Information S1). The phase delay of velocity changes with respect to the M_2 tide is expressed in the Supporting Information S1 (refer to Text S4).

Based on the velocity variations, dv/v, related to the M_2 tide and maximum volumetric strain of the M_2 tide, ε, on the ground surface computed by GOTIC2, we can infer the strain–velocity sensitivity, $\frac{dv/v}{\varepsilon}$, at each station. Figure 3 illustrates the spatial distribution of strain– velocity sensitivity. Sensitivity values ranged from approximately 10^3 to 10^5, which is consistent with the range of values (2.3×10^3 to 6.9×10^4) obtained in the shallow portion of the crust by previous studies (Hillers et al., 2015; Sens-Schönfelder & Eulenfeld, 2019; Takano et al., 2014, 2019). Although the seismic velocity variations at each station were independently evaluated, the spatial distribution of the tidal response of the velocity variations displayed a characteristic spatial pattern. In addition, the spatial distributions of the tidal response of the velocity variations were compared with the geological setting of the Japanese islands. The locations of the active faults obtained from the digital map (Nakata & Imaizumi, 2002) and active volcanoes are presented in Figure 1b. First, a large tidal response was observed in the Kyushu region, where active volcanoes along the Ryukyu arc volcanic front and the Median Tectonic Line (MTL) were located. Certain stations in the Shikoku region, intersecting with the MTL, exhibited a large tidal response to velocity variations. The regions spanning from central Japan to the Kinki region, where several active seismic faults have been detected, were characterized by large tidal responses. Although the southern portion of the Chubu region facing the Pacific Ocean exhibits a small tidal strain, it produced a larger tidal strain response than the surrounding area. In Kanto and the eastern portion of the Chubu region, a large tidal response of velocity variations was observed in the area east of the Niigata-Kobe
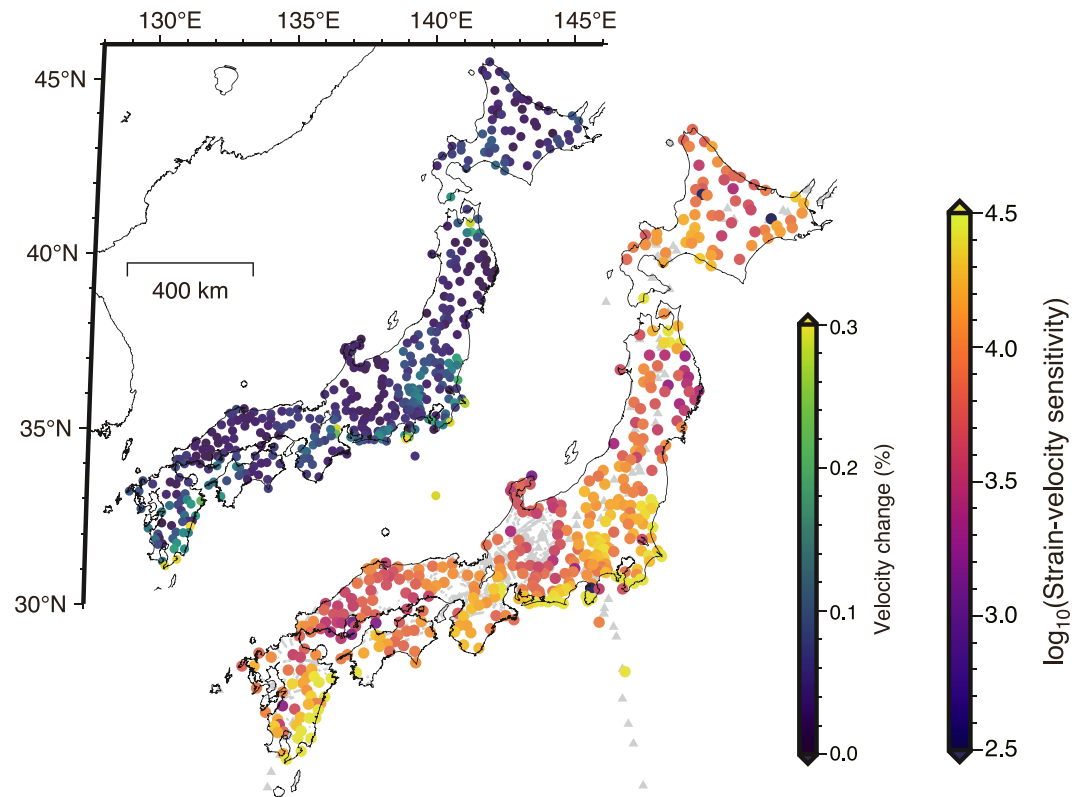
Figure 3. Spatial distribution of velocity variations in response to the M_2 tide (top map) and tidal strain response of velocity variations (bottom map). The stations with Akaike Information Criterion increments less than 0 are plotted as circles. The gray triangles and lines in the lower-right map display active volcanoes and active faults, respectively.
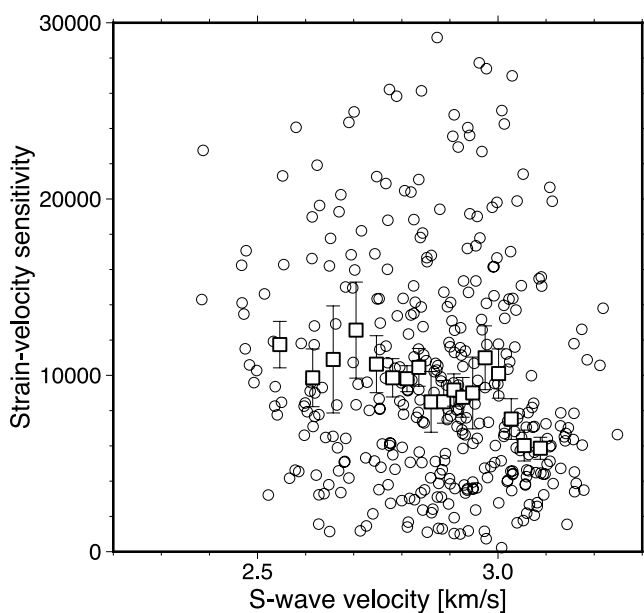
Figure 4. Relationship between S-wave velocity at depth of 1 km, and strain–velocity sensitivity at each station. White circles depict strain–velocity sensitivity at each station, and squares portray the mean of 100 bootstrap-resamplings of strain–velocity sensitivity for bins of 0.06 km/s in S-wave velocity.

Tectonic Line, wherein a high strain rate was observed to be dominated by a large contraction in the WNW—ESE direction (Sagiya et al., 2000). In the Tohoku region, the back-arc area of the Tohoku region generated a slightly larger tidal response than the island arc area of the region. In particular, the northern tip of the Tohoku region displayed a large tidal response. Moreover, a small tidal response to the velocity variations was observed in the central region of Hokkaido. However, the tidal response of the velocity variations was not strongly correlated with the geological features.

To systematically investigate the characteristics of velocity variations in response to the tide, we compared the strain–velocity sensitivity with the S-wave velocity structure estimated from the cross-correlations of microseisms using Hi-net seismic stations (Nishida et al., 2008). From the depth sensitivities of surface waves within the frequency band of 0.2–0.5 Hz, the noise correlations observed in this study are concentrated on the depth of a few kilometers (Figure S5 in Supporting Information S1). We here compared the strain–velocity sensitivity with the S-wave velocity from the depth at which the sensor was deployed to a depth of 1 km. The strain–velocity sensitivity against the S-wave velocity at each seismic station is presented in Figure 4. For each bin, the average strain–velocity sensitivity increased linearly as the S-wave velocity decreased. However, the tidal strain response of the velocity varied considerably. Although the variations in the tidal response at the same S-wave velocity may be caused by various geomaterials, the statistical trend of the tidal response suggested certain common physical characteristics. Notably, the tomographic model of S-wave velocity and the

autocorrelation function in this study has a different spatial resolution. At certain stations, the region in which the autocorrelation function propagated does not necessarily correspond to the S-wave velocity structure estimated by cross-correlation functions of ambient noise, which may alter the relationship between the strain and velocity sensitivity and S-wave velocity.

5. Discussion

We utilized a state-space model to extract the tidal responses of velocity variations. The resulting tidal responses displayed a characteristic spatial pattern, with the strain-velocity sensitivity showing a tendency to increase in regions of low S-wave velocity within the shallow crust. The mechanism through which the seismic velocities respond to deformations is commonly interpreted as the opening and closing of microcracks in a medium (Walsh, 1965). If the rock strain indicates a nonhysteresis function of the confining pressure P_c and pore pressure P_o, the strain sensitivity of the velocity variations in the grain material can be formulated assuming a small aspect ratio, such as follows Shapiro (2003):

$$\frac{1}{V_{S_0}}\frac{\partial V_S}{\partial \varepsilon} \sim \frac{1}{2\gamma^2}\phi_{c_0}\exp\left(-\frac{1}{\gamma}CP\right) \tag{6}$$

where γ represents the aspect ratio of the pore, V_{S_0} denotes the S-wave velocity in a static state, ϕ_{c_0} represents the porosity of intergranular pore defined as compliant porosity, C indicates the drained compressibility and P represents the effective pressure. The effective pressure is defined in terms of the pore pressure P_o and confining pressure P_c as follows:

$$P = P_c - P_o. \tag{7}$$

As related in Equation 6, the strain sensitivity decreases with the increasing effective pressure. According to Equation 6, the aspect ratio of pores along with the pore pressure and porosity of the intergranular pores contribute to the strain–velocity sensitivity. The contribution of these parameters can complicate the relationship between the S-wave velocity and the tidal strain response, as shown in Figure 4. Thus, a detailed comparison of the strain–velocity sensitivities with the structure of the crust other than S-wave velocity is required to investigate the extent to which each factor contributes to the observed strain–velocity sensitivities. V_P/V_S in the rocks is sensitive to liquid compressibility, pore geometry, and liquid volume fraction. In contrast, the ratio of the fractional variations in V_S and V_P is sensitive to liquid compressibility and pore geometry (Takei, 2002). Upon comparing the present findings with V_P/V_S and the ratio of the fractional variations in V_S and V_P, we can employ the constraints on these crustal parameters.

Brenguier et al. (2014) estimated the seismic velocity susceptibility to the dynamic stress induced by the 2011 Tohoku-Oki earthquake. They interpreted the spatial distributions of the large susceptibilities of seismic velocity based on the highly pressurized fluid situated beneath the active volcanoes in eastern Japan. However, the tidal strain response of the velocity variations surrounding the volcanic front in eastern Japan was not large. The wavefield of autocorrelations is sensitive down to a depth of a few kilometers (Figure S5 in Supporting Information S1), which is shallower than the depth sensitivity reported by Brenguier et al. (2014). In particular, the noise autocorrelation can be interpreted as observing more local structural changes than the cross-correlation analysis. The S-wave velocity structure inferred from the cross-correlations of microseisms (Nishida et al., 2008) situated 1 km beneath the volcanic front is not low in comparison with that of other regions because the spatial resolution of the correlations does not delineate the small-scale velocity perturbation of the magma chamber (Nagaoka et al., 2012). As the Hi-net stations are sparsely located in volcanic regions, the autocorrelation analysis would provide only a small sample of information beneath volcanoes. This study lacked a sample of the tidal response of the velocity variations beneath volcanoes and may have analyzed a different region than Brenguier et al. (2014). Therefore, differences may appear in the spatial distribution of the tidal response and the seismic stress susceptibility. Brenguier et al. (2014) assessed the transient response of the crust to the earthquake, whereas our results demonstrated the crustal response to the semi-diurnal static strain changes. In the future, researchers need to consider both the transient and static responses of the crust to more comprehensively understand the mechanical properties of the crust in response to strain or stress.

6. Conclusions

In this study, we examined the seismic velocity variations in response to tides throughout Japan. Utilizing the dense seismic network in Japan, we investigated the spatial extent of the tidal strain–velocity sensitivities. Accordingly, we extracted the tidal responses of velocity variations from the hourly stacked noise autocorrelations by combining the extended Kalman filter with the Maximum Likelihood method. The strain–velocity sensitivities varied from approximately 10^3 to 10^5. Upon comparing the strain–velocity sensitivity with the S-wave velocity structure in Japan, the tidal response to seismic velocity variations was larger at low S-wave velocities in the shallow crust. Based on the strain–velocity relationship in the grain material, the current results implied that the spatial variations in the tidal response of seismic wave velocity can potentially characterize the fluid pressure or shape of pores in the crust. As the tides and seismic ambient noise can be observed at any location and instant, the flexibility of the state-space model will enable us to attain a higher spatial resolution of the tidal strain–velocity sensitivities with a dense seismic network, such as a Large N-array or Distributed Acoustic Sensing observation. The tidal responses of velocity variations in various time periods also will be extracted to investigate the temporal variations in the mechanical properties of the shallow crust.

Data Availability Statement

We used data from Hi-net (https://doi.org/10.17598/nied.0003) managed by the National Research Institute for Earth Science and Disaster Prevention (NIED), Japan. The Python code of the extended Kalman filter is also available on the Zenodo web page (https://zenodo.org/record/7476091#.Y8_BluzP20p).

References

Akaike, H. (1974). A new look at the statistical model identification. *IEEE Transactions on Automatic Control*, *19*(6), 716–723. https://doi.org/10.1109/tac.1974.1100705

Beyreuther, M., Barsch, R., Krischer, L., Megies, T., Behr, Y., & Wassermann, J. (2010). ObsPy: A python toolbox for seismology. *Seismological Research Letters*, *81*(3), 530–533. https://doi.org/10.1785/gssrl.81.3.530

Brenguier, F., Campillo, M., Hadziioannou, C., Shapiro, N. M., Nadeau, R. M., & Larose, E. (2008). Postseismic relaxation along the San Andreas Fault at parkfield from continuous seismological observations. *Science*, *321*(5895), 1478–1481. https://doi.org/10.1126/science.1160943

Brenguier, F., Campillo, M., Takeda, T., Aoki, Y., Shapiro, N., Briand, X., et al. (2014). Mapping pressurized volcanic fluids from induced crustal seismic velocity drops. *Science*, *345*(6192), 80–82. https://doi.org/10.1126/science.1254073

Brenguier, F., Shapiro, N. M., Campillo, M., Ferrazzini, V., Duputel, Z., Coutant, O., & Nercessian, A. (2008). Towards forecasting volcanic eruptions using seismic noise. *Nature Geoscience*, *1*(2), 126–130. https://doi.org/10.1038/ngeo104

Cartwright, D., & Edden, A. C. (1973). Corrected tables of tidal harmonics. *Geophysical Journal International*, *33*(3), 253–264. https://doi.org/10.1111/j.1365-246x.1973.tb03420.x

De Fazio, T. L., Aki, K., & Alba, J. (1973). Solid Earth tide and observed change in the in situ seismic velocity. *Journal of Geophysical Research*, *78*(8), 1319–1322. https://doi.org/10.1029/jb078i008p01319

Durbin, J., & Koopman, S. J. (2012). *Time series analysis by state space methods* (Vol. 38). Oxford University Press.

Hillers, G., Retailleau, L., Campillo, M., Inbal, A., Ampuero, J.-P., & Nishimura, T. (2015). In situ observations of velocity changes in response to tidal deformation from analysis of the high-frequency ambient wavefield. *Journal of Geophysical Research: Solid Earth*, *120*(1), 210–225. https://doi.org/10.1002/2014jb011318

Hobiger, M., Wegler, U., Shiomi, K., & Nakahara, H. (2014). Single-station cross-correlation analysis of ambient seismic noise: Application to stations in the surroundings of the 2008 Iwate-Miyagi Nairiku earthquake. *Geophysical Journal International*, *198*(1), 90–109. https://doi.org/10.1093/gji/ggu115

Maeda, T., Obara, K., Furumura, T., & Saito, T. (2011). Interference of long-period seismic wavefield observed by the dense hi-net array in Japan. *Journal of Geophysical Research*, *116*(B10), B10303. https://doi.org/10.1029/2011jb008464

Mao, S., Campillo, M., van der Hilst, R. D., Brenguier, F., Stehly, L., & Hillers, G. (2019). High temporal resolution monitoring of small variations in crustal strain by dense seismic arrays. *Geophysical Research Letters*, *46*(1), 128–137. https://doi.org/10.1029/2018gl079944

Matsumoto, K., Sato, T., Takanezawa, T., & Ooe, M. (2001). GOTIC2: A program for computation of oceanic tidal loading effect. *Journal of the Geodetic Society of Japan*, *47*(1), 243–248.

Nagaoka, Y., Nishida, K., Aoki, Y., Takeo, M., & Ohminato, T. (2012). Seismic imaging of magma chamber beneath an active volcano. *Earth and Planetary Science Letters*, *333*, 1–8. https://doi.org/10.1016/j.epsl.2012.03.034

Nakata, T., & Imaizumi, T. (2002). *Digital active fault map of Japan*. University of Tokyo Press.

Nishida, K., Kawakatsu, H., & Obara, K. (2008). Three-dimensional crustal S wave velocity structure in Japan using microseismic data recorded by Hi-net tiltmeters. *Journal of Geophysical Research*, *113*(B10), B10302. https://doi.org/10.1029/2007jb005395

Nishida, K., Mizutani, Y., Ichihara, M., & Aoki, Y. (2020). Time-lapse monitoring of seismic velocity associated with 2011 Shinmoe-dake eruption using seismic interferometry: An extended Kalman filter approach. *Journal of Geophysical Research: Solid Earth*, *125*(9), e2020JB020180. https://doi.org/10.1029/2020jb020180

Obermann, A., & Hillers, G. (2019). Seismic time-lapse interferometry across scales. *Advances in geophysics* (Vol. 60, pp. 65–143). Elsevier.

Reasenberg, P., & Aki, K. (1974). A precise, continuous measurement of seismic velocity for monitoring in situ stress. *Journal of Geophysical Research*, *79*(2), 399–406. https://doi.org/10.1029/jb079i002p00399

Sagiya, T., Miyazaki, S., & Tada, T. (2000). Continuous GPS array and present-day crustal deformation of Japan. *Pure and Applied Geophysics*, *157*(11), 2303–2322. https://doi.org/10.1007/pl00022507

Sens-Schönfelder, C., & Eulenfeld, T. (2019). Probing the in situ elastic nonlinearity of rocks with Earth tides and seismic noise. *Physical Review Letters*, *122*(13), 138501. https://doi.org/10.1103/physrevlett.122.138501

Shapiro, S. A. (2003). Elastic piezosensitivity of porous and fractured rocks. *Geophysics*, *68*(2), 482–486. https://doi.org/10.1190/1.1567215

Takagi, R., Nishida, K., Aoki, Y., Maeda, T., Masuda, K., Takeo, M., et al. (2015). A single bit matters: Coherent noise of seismic data loggers. *Seismological Research Letters*, *86*(3), 901–907. https://doi.org/10.1785/0220150030

Takano, T., Nishimura, T., & Nakahara, H. (2017). Seismic velocity changes concentrated at the shallow structure as inferred from correlation analyses of ambient noise during volcano deformation at Izu-Oshima, Japan. *Journal of Geophysical Research: Solid Earth*, *122*(8), 6721–6736. https://doi.org/10.1002/2017jb014340

Takano, T., Nishimura, T., Nakahara, H., Ohta, Y., & Tanaka, S. (2014). Seismic velocity changes caused by the Earth tide: Ambient noise correlation analyses of small-array data. *Geophysical Research Letters*, *41*(17), 6131–6136. https://doi.org/10.1002/2014gl060690

Takano, T., Nishimura, T., Nakahara, H., Ueda, H., & Fujita, E. (2019). Sensitivity of seismic velocity changes to the tidal strain at different lapse times: Data analyses of a small seismic array at Izu-Oshima volcano. *Journal of Geophysical Research: Solid Earth*, *124*(3), 3011–3023. https://doi.org/10.1029/2018jb016235

Takei, Y. (2002). Effect of pore geometry on V_p/V_s: From equilibrium geometry to crack. *Journal of Geophysical Research*, *107*(B2), 2043. https://doi.org/10.1029/2001jb000522

Van Der Walt, S., Colbert, S. C., & Varoquaux, G. (2011). The NumPy array: A structure for efficient numerical computation. *Computing in Science & Engineering*, *13*(2), 22–30. https://doi.org/10.1109/mcse.2011.37

Virtanen, P., Gommers, R., Oliphant, T. E., Haberland, M., Reddy, T., Cournapeau, D., et al. (2020). SciPy 1.0: Fundamental algorithms for scientific computing in python. *Nature Methods*, *17*(3), 261–272. https://doi.org/10.1038/s41592-019-0686-2

Walsh, J. (1965). The effect of cracks on the uniaxial elastic compression of rocks. *Journal of Geophysical Research*, *70*(2), 399–411. https://doi.org/10.1029/jz070i002p00399

Weaver, R. L., & Lobkis, O. I. (2000). Temperature dependence of diffuse field phase. *Ultrasonics*, *38*(1–8), 491–494. https://doi.org/10.1016/s0041-624x(99)00047-5

Wessel, P., & Smith, W. H. (1998). New, improved version of generic mapping tools released. *Eos, Transactions American Geophysical Union*, *79*(47), 579. https://doi.org/10.1029/98eo00426

Yamamura, K., Sano, O., Utada, H., Takei, Y., Nakao, S., & Fukao, Y. (2003). Long-term observation of in situ seismic velocity and attenuation. *Journal of Geophysical Research*, *108*(B6), 2317. https://doi.org/10.1029/2002jb002005

Zhu, C., Byrd, R. H., Lu, P., & Nocedal, J. (1997). Algorithm 778: L-BFGS-B: Fortran subroutines for large-scale bound-constrained optimization. *ACM Transactions on Mathematical Software*, *23*(4), 550–560. https://doi.org/10.1145/279232.279236